

See discussions, stats, and author profiles for this publication at: <https://www.researchgate.net/publication/263666366>

# Tin quantum Dots embedded in nitrogen-doped carbon nanofibers As excellent anode for lithium-ion batteries

ARTICLE *in* NANO ENERGY · OCTOBER 2014

Impact Factor: 10.33 · DOI: 10.1016/j.nanoen.2014.06.030

---

CITATIONS

11

READS

52

## 8 AUTHORS, INCLUDING:



Guanhua Zhang

Hunan University

18 PUBLICATIONS 327 CITATIONS

[SEE PROFILE](#)



Feng Li

Kunming University of Science and Technol...

151 PUBLICATIONS 3,112 CITATIONS

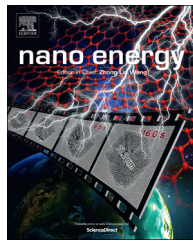
[SEE PROFILE](#)



Available online at www.sciencedirect.com

ScienceDirect

journal homepage: www.elsevier.com/locate/nanoenergy



RAPID COMMUNICATION

# Tin quantum dots embedded in nitrogen-doped carbon nanofibers as excellent anode for lithium-ion batteries

Guanhua Zhang<sup>a</sup>, Jian Zhu<sup>a</sup>, Wei Zeng<sup>a</sup>, Sucheng Hou<sup>a</sup>, Feilong Gong<sup>b</sup>, Feng Li<sup>b</sup>, Cheng Chao Li<sup>a,\*</sup>, Huigao Duan<sup>a,\*</sup>

<sup>a</sup>College of Physics and Microelectronics, State Key Laboratory for Chemo/Biosensing and Chemometrics, Hunan University, Changsha 410082, China

<sup>b</sup>State Laboratory of Surface and Interface Science and Technology, Zhengzhou University of Light Industry, Zhengzhou 450002, China

Received 17 May 2014; received in revised form 18 June 2014; accepted 26 June 2014  
Available online 5 July 2014



## KEYWORDS

Sn quantum dots;  
N-doped carbon  
nanofibers;  
Electrospinning;  
Anode;  
Li-ion battery

## Abstract

Sn/C composites with sub-10-nm-scale tin nanoparticles uniformly dispersed in a carbon matrices are believed to be excellent anode materials for high energy and power density lithium-ion batteries. However, it is difficult to incorporate high-capacity, active Sn into the carbon structures due to the hydrophobic nature of the carbon surface. Surfactants and/or templates are always required for uniform dispersion of active Sn, inevitably increasing the production cost and degrading the electronic conductivity. In this work, we reported a facile and scalable electrospinning technology to synthesize Sn quantum dots finely embedded in N-doped carbon nanofibers. The composite electrode exhibited a high reversible capacity of 887 mAh g<sup>-1</sup> at a current density of 0.1 A g<sup>-1</sup> after 200 cycles, about 75% retention of the initial capacity. Moreover, it showed good rate capability even when cycled at 0.2 A g<sup>-1</sup> about 685 mAh g<sup>-1</sup> after 500 cycles and 508 mAh g<sup>-1</sup> at 0.4 A g<sup>-1</sup> after 200 cycles. The exceptional performance is supposed to benefit from the high electric conductivity of N-doped porous carbon nanofiber structures, which not only provides fast and versatile transport pathways for the electrolyte ions and electrons, but also simultaneously solves the major problems of pulverization, loss of electrical contact, and particle aggregation of Sn anode. Moreover, the short diffusion path for both electrons and ions provided by the ultrasmall Sn particles further improved the rate performance.

© 2014 Elsevier Ltd. All rights reserved.

\*Corresponding authors.

E-mail addresses: ghzhang2012@126.com (G. Zhang), licc@hnu.edu.cn (C.C. Li), duanhg@hnu.edu.cn (H. Duan).

## Introduction

Development in automobile market is presently aimed at producing low emission cars, such as zero emission electric vehicles (EVs) and hybrid electric vehicles (HEV). Suitable energy storage devices are the key parts of electric vehicles (EVs) and high-energy storage lithium ion batteries (LIBs) are considered as ideal candidates [1-3]. To make these batteries appropriate for EVs applications, more improvements are necessary in terms of energy density, cycle life and capacity retention. Pure metallic Sn has attracted considerable attention as an anode material for LIBs owing to its high theoretical specific capacity ( $992 \text{ mA h g}^{-1}$  or  $7262 \text{ mA h cm}^{-3}$  for  $\text{Li}_{4.4}\text{Sn}$ ), which is almost 3 times higher than that of commercialized graphite ( $372 \text{ mA h g}^{-1}$  for  $\text{LiC}_6$ ) [1,4], and its high operating voltage along with the absence of solvent intercalation [2,5,6]. Unfortunately, the huge volumetric expansion and aggregation of Sn nanoparticles (NPs) during lithium alloying and dealloying processes lead to severe degradation of the electrodes upon cycling and dramatically shorten the cycle life of the Sn electrode [1-6]. Therefore, it is still a huge challenge to further improve or optimize the electrochemical performance of the Sn electrode.

To overcome these issues, considerable efforts have been made to improve the structural stability and integrity of Sn anodes [7-9]. It is believed that two strategies are feasible. The first is the fabrication of uniformly dispersed nano-Sn in a conductive matrix (such as carbon) to accommodate volume change and maintain the mechanical integrity of the composite electrode [3,5,8-11]. The second strategy to enhance the electrochemical performance is to reduce the particle size of Sn to sub-10-nm scale to form quantum dots (QDs), which may efficiently mitigate the absolute strain induced by the large volume change during lithiation/delithiation, and retard particle pulverization. Definitely, a Sn/C composite with uniform sub-10-nm-scale tin NPs dispersed in a carbon matrix would be a promising anode for LIBs. For instance, Scrosati and co-workers synthesized a nanostructured Sn/C composite which could provide a stable capacity of  $500 \text{ mAh g}^{-1}$  over more than 200 cycles [12]. The carbon matrices not only acted as a buffer to accommodate the volume expansion, but also prevented the aggregation of Sn NPs. Moreover, Xu's group demonstrated that Sn nanograin uniformly dispersed in spherical conductive carbon matrices still contained a reversible capacity of  $710 \text{ mA h g}^{-1}$  after 130 cycles at  $0.2 \text{ A g}^{-1}$  [9]. The remarkable performance is attributed to the small particle size ( $\sim 10 \text{ nm}$ ) and continuous path for Li ions and electrons inside the nano-Sn/C composite spheres. More recently, ultrasmall Sn NPs ( $\sim 5 \text{ nm}$ ) embedded in nitrogen-doped porous carbon network has been synthesized from the organic framework, delivering a capacity of  $722 \text{ mA h g}^{-1}$  after 200 cycles at the current density of  $0.2 \text{ A g}^{-1}$  [8]. Although various synthetic routes have been successfully developed for nano-Sn/C composite, it should be noted most of these products are irregular particles with relatively large size.

One-dimensional (1D) carbon nanoarchitectures such as nanotubes (NTs) [13,14], nanowires (NWs) [1,15], nanorods (NRs) [16-18] and nanofibers (NFs) [19-21] are proven to have much better kinetic properties than reported carbon

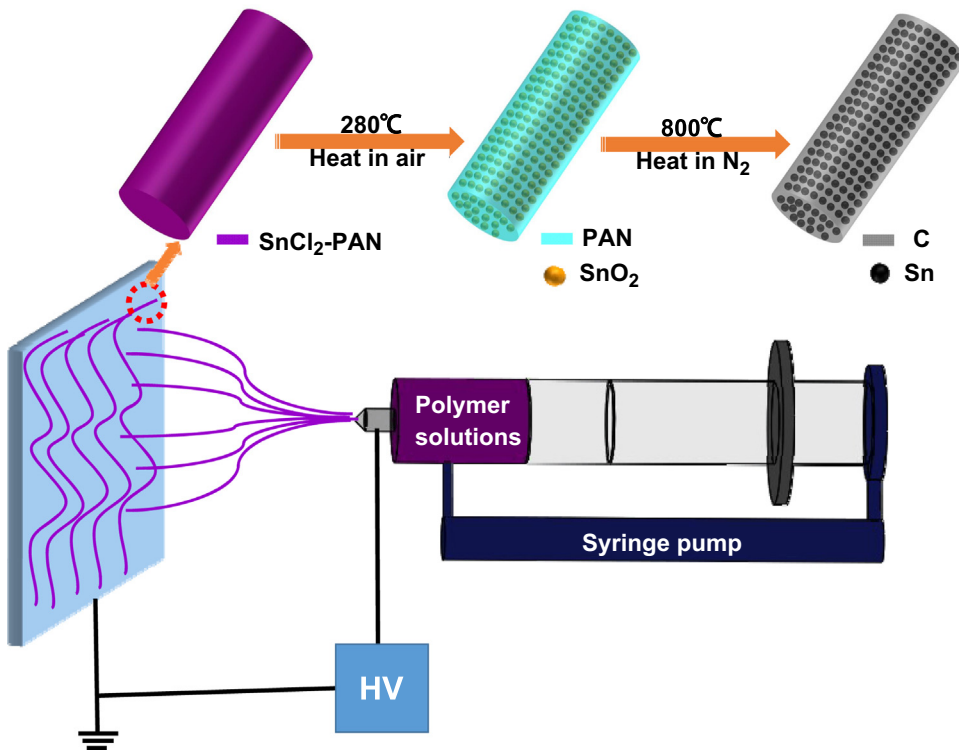
matrixes with particle morphology. Their uniform structure, orientated electronic and ionic transport path and strong tolerance to stress change can enable efficient transport of both Li-ions and electrons [19]. However, it is difficult to incorporate high-capacity, active Sn into these 1D carbon structures due to the hydrophobic nature of the carbon surface. Surfactants and/or templates are always required for uniform dispersion, inevitably increasing the production cost and degrading the electronic conductivity [19,22]. Hence, it is desirable to synthesize uniform dispersion Sn QDs within conductive CNFs supports that not only retains the high capacity of the nanosized material but also shows excellent cycling performance by avoiding excessive sub-reactions and aggregation of Sn.

Herein, we reported a facile, straightforward method to synthesize of Sn QDs finely embedded in N-doped CNFs by the electrospinning technique followed by annealing under nitrogen. Compared to other reported Sn/C nanocomposites [1,11,12,14,20,23-25], our sub-5-nm Sn QDs can further enhance Li ion insertion by reducing diffusion/migration barrier and allow easy penetration of the electrolyte between neighboring NPs and hence reduce internal resistance, which is particularly helpful for high energy/power applications. Moreover, the N-doped carbon matrices with high electric conductivity could provide extra "cushion" for the structure to accommodate large volume change induced by Li-Sn alloying/dealloying reactions. This newly designed Sn QDs@CNFs displayed extraordinary LIBs performance with outstanding reversible capacity, excellent capacity retention, high Coulombic efficiency, good rate capability and superior cyclic performance, highlighting the importance of the unique combination of ultrasmall Sn QDs and CNFs matrices to overcome the aforementioned problems and achieve the maximum electrochemical performance. We demonstrated the discharge capacity up to 200 cycles with  $887 \text{ mAh g}^{-1}$  at a current density of  $0.1 \text{ A g}^{-1}$ , and  $508 \text{ mAh g}^{-1}$  at  $0.4 \text{ A g}^{-1}$ .

## Experimental

### Synthesis

All the chemicals were of analytical grade and used as received without further purification. Typically,  $0.8 \text{ g}$  of polyacrylonitrile (PAN, Mw=150,000, Sigma) was dissolved in  $10 \text{ mL}$  of N, N-dimethylformamide (DMF, Tianjin Chemicals, 99.0%), and then  $0.28 \text{ g}$  of Tin(II) chloride dihydrate ( $\text{SnCl}_2 \cdot 2\text{H}_2\text{O}$ , 98.5% purity, National Medicine Co., Ltd., Shanghai, China) was added to form a mixed solution. After vigorous stirring for  $4 \text{ h}$  at  $60^\circ\text{C}$ , buff and sticky polymer solution was obtained for the subsequent electrospinning process. As for a typical electrospinning process (shown in Scheme 1), the spinneret had an inner diameter of  $0.6 \text{ mm}$ . Grounded aluminum strips ( $20 \text{ cm}$  in width) with parallel gaps of about  $1 \text{ cm}$  were used as collectors. A distance of  $15 \text{ cm}$  and a direct current voltage of  $18 \text{ kV}$  were maintained between the tip of the spinneret and the collector. The as-electrospinning  $\text{SnCl}_2/\text{PAN}$  nanofibers (denoted as  $\text{SnCl}_2\text{-PAN}$ ) were dried for  $24 \text{ h}$  in vacuum at  $60^\circ\text{C}$ . The dried  $\text{SnCl}_2\text{-PAN}$  were further annealed in an air-circulated oven at  $280^\circ\text{C}$  for  $2 \text{ h}$  at a heating rate of  $2^\circ\text{C min}^{-1}$ , and then



**Scheme 1** Schematic illustration of electrospinning process of Sn QDs@CNFs.

annealed in a  $\text{N}_2$  flow at  $800\text{ }^\circ\text{C}$  for 1 h at a heating rate of  $5\text{ }^\circ\text{C min}^{-1}$ . The annealed product was designated as Sn QDs@CNFs. The preparation process of the N-doped CNFs was the same as the method of Sn QDs@CNFs, just without the addition of  $\text{SnCl}_2 \cdot 2\text{H}_2\text{O}$ .

## Characterization

The as-prepared products were characterized by a powder X-ray diffraction (XRD, Siemens D-5000) with  $\text{Cu K}\alpha$  ( $\lambda = 0.15418\text{ nm}$ ). The morphology of the synthesized samples was examined using field-emission scanning electron microscopy (SEM, Hitachi S-4800) and transmission electron microscopy (TEM, JEOL JEM 2100) operated at an accelerating voltage of  $200\text{ kV}$ . The Raman spectra were obtained on a Renishaw Invia Raman spectrometer with a solid-state laser ( $632.8\text{ nm}$ ) operated at room temperature. Thermo-gravimetric and differential thermal analyses (TG/DTA) were carried out using a Shimadzu DTG-60 thermal analyzer at a heating rate of  $5\text{ }^\circ\text{C min}^{-1}$  in air.

## Electrochemical measurements

A CR2025-type coin cell was assembled to investigate the electrochemical properties of the products. The working electrodes were prepared by mixing 80 wt% active material, 10 wt% acetylene black (Super-P), and 10 wt% binder (LA133 and CMC) in distilled water and absolute alcohol mixture. After coating the above slurries on a copper foil (with the loading of the active material about  $1.8\text{--}2.0\text{ mg cm}^{-2}$ ), the electrodes were dried at  $80\text{ }^\circ\text{C}$  under vacuum to remove the solvent (3:2 by volume). The cells were assembled in an argon-filled glovebox (Mikrouna Universal 2440/750) with

water and oxygen contents less than 1 ppm. A Celgard 2400 microporous polypropylene membrane was used as a separator. The electrolyte consisted of a solution of 1 M  $\text{LiPF}_6$  in ethylene carbonate/dimethyl carbonate/diethyl carbonate (1:1:1, in weight percent). Pure lithium foil was used as a counter-electrode. The discharge and charge measurements were carried out on an Arbin BT2000 system with the cut-off potentials being 0.02 and  $3\text{ V}$  at different current densities from  $0.1$  to  $0.4\text{ A g}^{-1}$ . The CV experiment was also tested on the Arbin battery test system at a scan rate of  $0.5\text{ mV s}^{-1}$ . Electrochemical impedance spectroscopy (EIS) was carried out on a CHI660e (Chenhua, Shanghai, China) electrochemical workstation in the frequency range of  $100\text{ kHz}$  to  $10\text{ mHz}$  at a fixed perturbation amplitude of  $5\text{ mV}$ .

## Results and discussion

**Figure 1a** shows the XRD patterns of the Sn QDs@CNFs and N-doped CNFs. The sharp diffraction peaks at  $30^\circ$ ,  $32^\circ$ ,  $43^\circ$ ,  $44^\circ$ ,  $55^\circ$ ,  $62^\circ$ ,  $63^\circ$ ,  $64^\circ$ ,  $72^\circ$ ,  $73^\circ$  and  $79^\circ$  were ascribed to the (200), (101), (220), (211), (301), (112), (400), (321), (420), (411) and (312) diffraction peaks of Sn (JCPDS Card 04-0673). No intensive peak belonging to Sn-oxides was detected, demonstrating the Sn-oxides was reduced completely to form metallic Sn by a carbothermal reduction reaction. The broad diffraction peak near  $25^\circ$ , corresponding to the (002) crystallographic plane of graphite, indicated the graphitic structure of the carbon materials (JCPDS Card 13-0148). The graphitization of carbon materials was also supported by Raman spectrum (**Figure 1b**). As shown in **Figure 1b**, the stronger band at  $1338\text{ cm}^{-1}$  could be assigned to defect-induced structures of carbon (D band), while the weaker band at  $1590\text{ cm}^{-1}$  was an indicator of

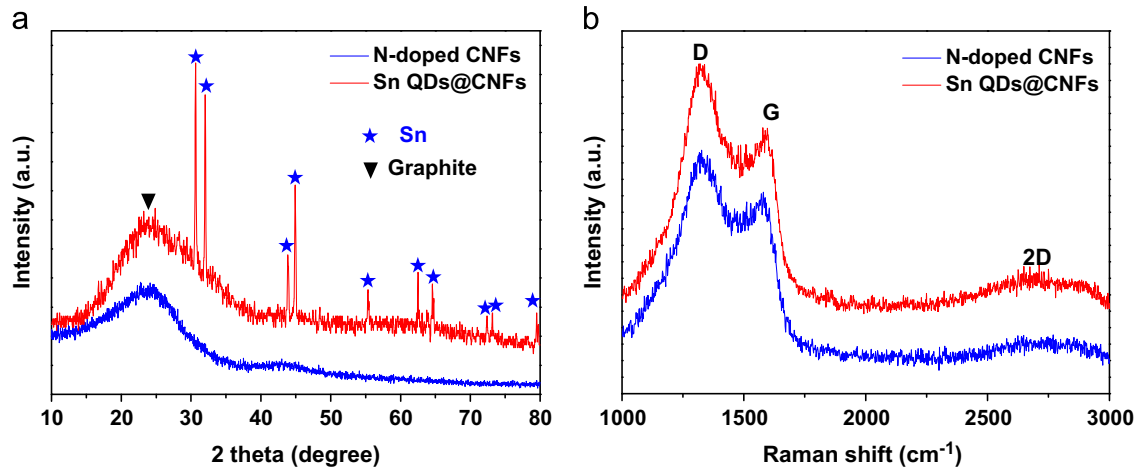


**Figure 1** (a) XRD patterns of Sn QDs@CNFs and N-doped CNFs; (b) Raman spectra of Sn QDs@CNFs and N-doped CNFs.

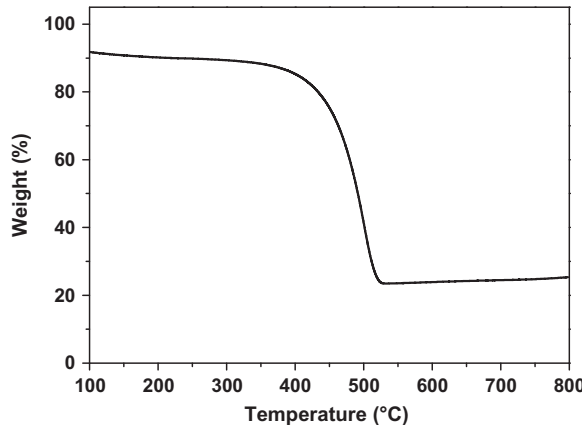


**Figure 2** Thermogravimetric analysis (TGA) of the Sn QDs@CNFs composite in air.

high-frequency E2g first-order graphitic crystallites (G band). Furthermore, the wide weaker 2D band centered at 2800 cm<sup>-1</sup> was associated with a second-order zone boundary phonon mode for graphene [24,26,27]. Moreover, the  $I_D/I_G$  ratio (1.22) of Sn QDs@CNFs was much higher than the one (1.16) of N-doped CNFs because of the anchored Sn NPs [28]. The results indicated that CNFs prepared under the designated carbonization conditions were amorphous carbon with disordered graphene sheets.

To gain insight into the chemical composition, thermogravimetric analysis (TGA) and differential thermal analysis (DTA) were performed on the Sn QDs@CNFs (Figure 2). The weight loss from 300 to 528 °C was mainly attributed to the carbon decomposition to carbon dioxide ( $C + O_2 \rightarrow CO_2$  (gas)), while the marginal weight increase at temperatures above 528 °C was attributed to the oxidation of Sn ( $Sn + O_2 \rightarrow SnO_2$ ). Assuming that the TGA heating finally produced  $SnO_2$ , the content of Sn QDs in the composite was determined to be 20% based on the following equation:

$$Sn (W\%) = 100 \times \frac{\text{molecular weight of Sn}}{\text{molecular weight of } SnO_2} \times \frac{\text{final weight of } SnO_2}{\text{initial weight of Sn QDs@CNFs}}$$

**Figure 3** shows the typical SEM images of the Sn QDs@CNFs. The ultralong NFs carbonized at 800 °C were indicated to several hundreds of micrometers (Figure 3a). Moreover, as can be seen from Figure 3b, the diameter distribution of the NFs was at about 210 nm. The high magnification image indicates the surface of the NFs was smooth (Figure 3c), and no Sn NPs were observed on the NFs in Figure 3d.

The detailed morphological and structural features of the NFs were also examined by TEM. Figure 4a shows a typical TEM image of Sn QDs@CNF. No aggregated Sn QDs were found on the surface, indicating that the particles were embedded in the CNFs. The high magnification TEM image (Figure 4b) reveals that uniform Sn QDs (black dots) were well dispersed in the CNFs. The lighter color in the NFs represents the carbon matrices and the darker color represents the metallic Sn QDs. In addition, we can also see that most of the Sn QDs were wrapped in the carbon matrices rather than exposed on the surface, being consistent with the SEM results. As a result, the carbon matrices not only prevented the aggregation of Sn particles, but also avoided the exfoliation of Sn QDs during lithiation/delithiation, maintaining the integrity of the whole electrode. To further explore the structure of the composites, high-resolution TEM (HRTEM) studies were carried out, as presented in Figure 4c. As ultrasmall Sn QDs were embedded in the CNFs, it was very difficult to observe the lattice spacing of the Sn crystal from the HRTEM. However, interestingly, a thin layer (~5 nm) of carbon was observed on the surface of the composites, and the lattice spacing was determined to be 0.34 nm, corresponding to the (002) planes of graphite, indicating that our CNFs contained well-graphitized structures. The presence and distribution of Sn elements were further verified by TEM line analysis (Figure 4d): Sn elements were shown to be uniformly distributed in the CNFs, along with the carbon and nitrogen elements. It is believed that N-doping can enhance the electric conductivity of carbon-based materials and thus could be beneficial to Li ion storage [8,13,19].

Intrigued by the unique structural features of Sn QDs@CNFs, we evaluated their lithium storage properties for potential application as an anode material in LIBs. Figure 5a shows the typical cyclic voltammograms (CVs) of Sn QDs@CNFs electrode in the initial five cycles at a scan rate of 0.5 mV s<sup>-1</sup> between 0 and 3 V. During the first cathodic sweep, the broad reduction

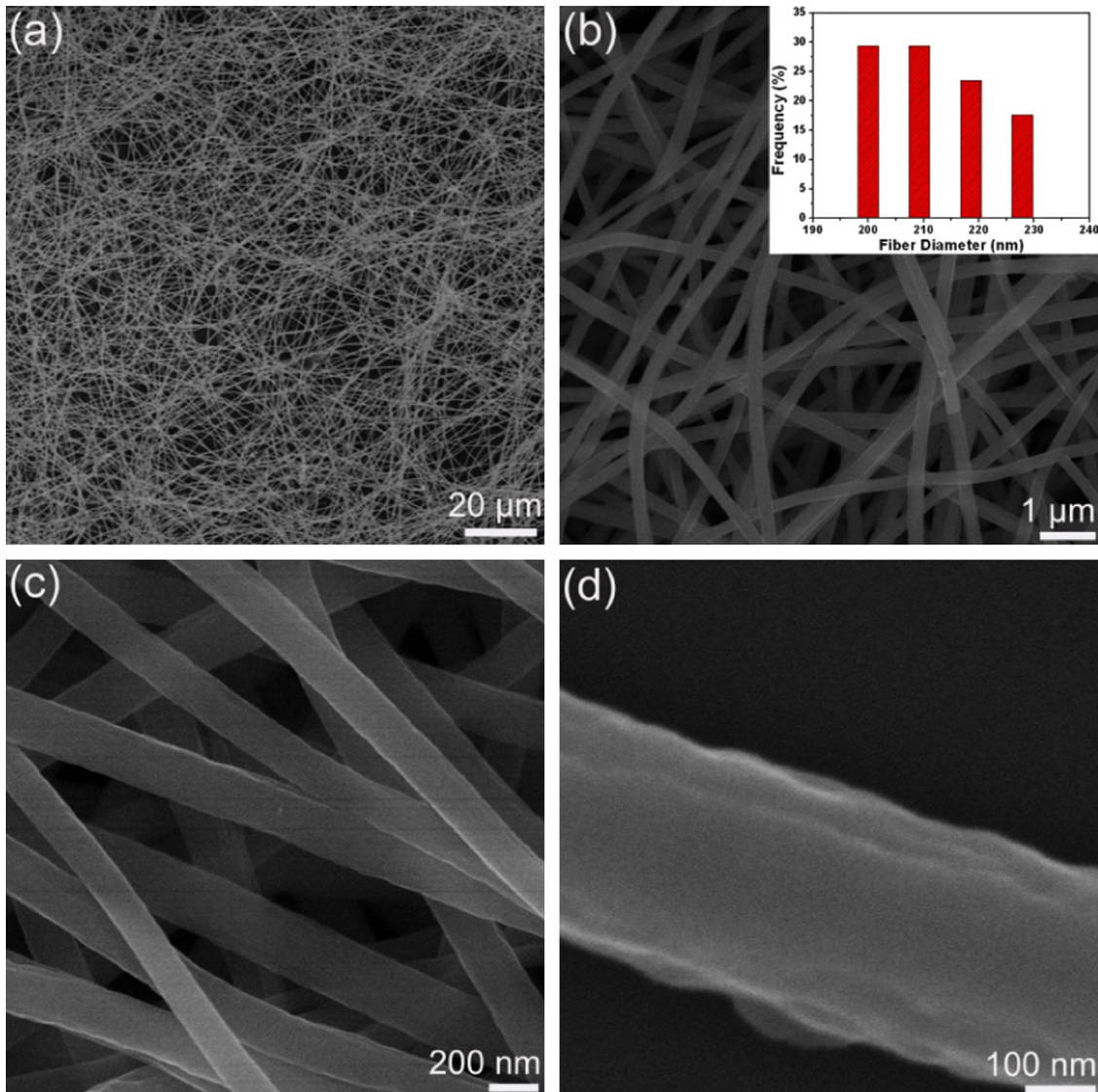


**Figure 3** SEM characterization of the morphologies of Sn QDs@CNFs. (a) SEM image of Sn QDs@CNFs, (b, c) the different magnification images and diameter distribution insets of Sn QDs@CNFs, and (d) high-magnification SEM image of a typical Sn QDs@CNF.

peak from 0.7 to 0.1 V was ascribed to both the occurrence of some irreversible reactions associated with the formation of an SEI film and  $\text{Li}_x\text{Sn}$  alloys ( $\text{Sn} + x\text{Li}^+ + xe^- \rightarrow \text{Li}_x\text{Sn}$ ,  $x \leq 4.4$ ), corresponding to the capacity loss during the first cycle [8,24]. Note that all peaks were reproducible and stable from the second cycle onward, implying excellent reversibility of the electrochemical reactions of the Sn QDs@CNFs electrode. Additionally, the CV curves are consistent with the previous reports on Sn/C composite anodes [8,9,24,25], indicating a similar electrochemical reaction occurred. Furthermore, the absence of peaks associated with the catalytic decomposition of the electrolyte on metallic Sn (at 1.05 or 1.55 V) implies that Sn QDs were perfectly embedded in the CNFs [8,24,25].

Typical galvanostatic charge/discharge profiles of the Sn QDs@CNFs electrode between 0.01 and 3 V at a current density of  $0.1 \text{ A g}^{-1}$  are shown in Figure 5b. The Sn QDs@CNFs electrode showed a high initial discharge capacity of approximately  $1176 \text{ mAh g}^{-1}$  and a lower capacity of

$910 \text{ mAh g}^{-1}$  in the second cycle, resulting in a first-cycle Coulombic efficiency of around 71%. The initial irreversible capacity loss was mainly associated with the inevitable formation of SEI and decomposition of electrolyte [8,17,25,29,30]. More importantly, the reversible capacity could maintain at  $\sim 887 \text{ mAh g}^{-1}$  after 200 cycles, about 75% retention of the initial capacity. The low shrinkage of charge/discharge curves after the first cycle implied the high cycling stability of the as-prepared composite. The Sn QDs could enhance Li ion insertion by reducing diffusion/migration barrier and allow easy penetration of the electrolyte between neighboring NPs. Moreover, the conductive N-doped carbon skeleton could not only provide extra “cushion” for the structure to accommodate large volume change induced by Li-Sn alloying/dealloying reactions but also supply ultrafast electronic transmission channels during the electrochemical process. Therefore, the combined advantages of the nanocomposite provided both the high

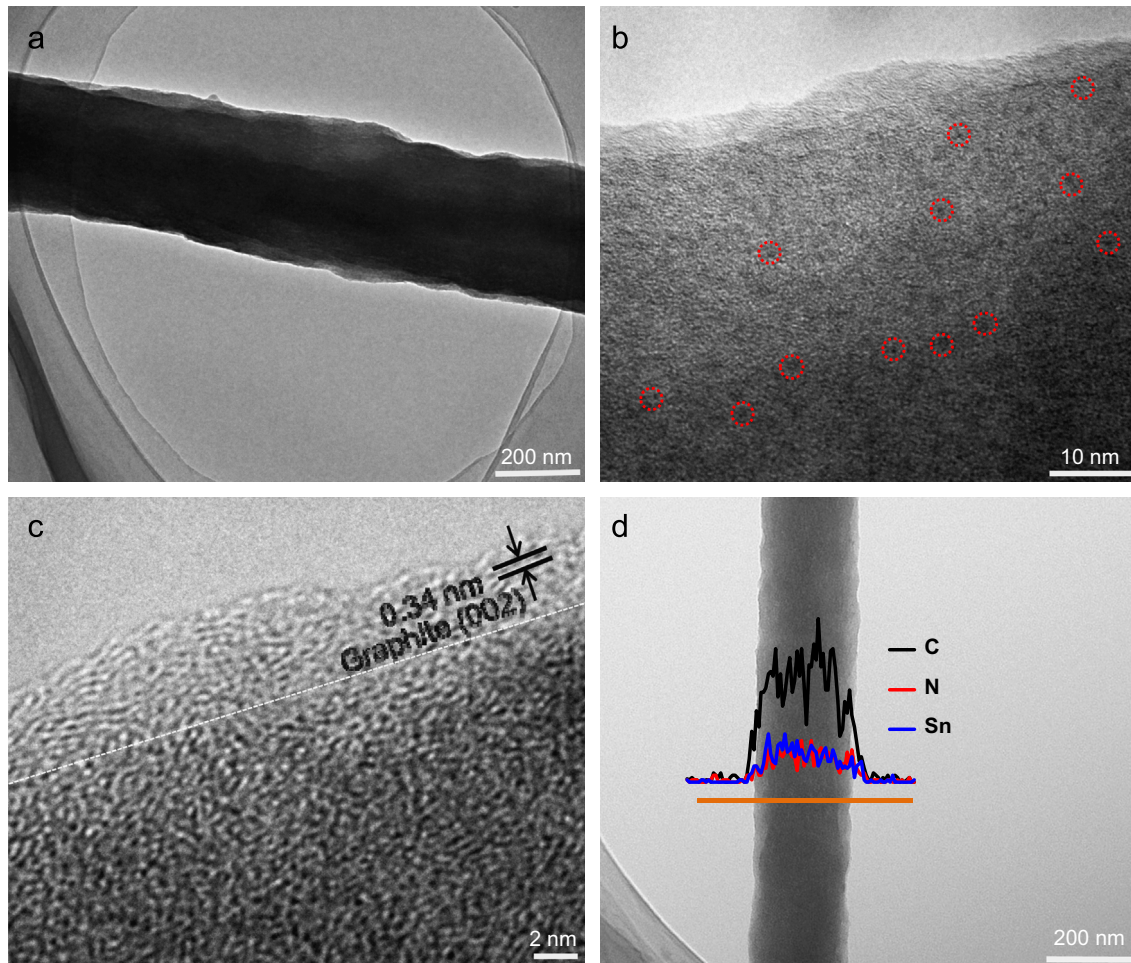


**Figure 4** TEM images of the synthesized nanostructures. (a, b) Low-magnification and high-magnification TEM images of Sn QDs@CNFs, (c) high-resolution image of Sn QDs@CNFs, and (d) TEM line analysis of Sn QDs@CNF.

capacity and the improved cycling stability. **Figure 5c** shows the cycling performance of the Sn QDs@CNFs composite during charge/discharge processes between 0.01 and 3 V at a current density of  $0.1 \text{ A g}^{-1}$ . The Sn QDs@CNFs exhibited exceptional cycling stability during 200 charge/discharge cycles with slight capacity decay in the first 10 cycles. The initial capacity fading might be derived from the partial irreversible insertion of lithium ions into the vacancies of the porous carbon matrices [8,31]. The Coulombic efficiency approached almost 100% after 10 cycles, showing excellent reversibility of the Sn QDs@CNFs. It is important to note that from the 100th cycle onwards, the discharge specific capacity displayed no decay but gradual increase, which might be ascribed to a gradual activation process (e.g. crystallinity degradation and amorphization) [24,28,32] and a “pseudo-capacitance-type behavior” (the reversible formation and decomposition of an organic polymeric/gel-like film from the electrolyte) [33–35] of the Sn QDs@CNFs electrode; similar phenomena were found in various Sn/C electrodes [24,28,36]. These results were also superior to those for Sn/C composites reported previously [5,12,25,37]. The excellent lithium storage properties and improved Coulombic efficiency could be attributed to the following reasons. The ultrasmall Sn QDs were thoroughly sealed in the CNFs; the carbon matrices accommodated the large volume

change and prevented Sn QDs aggregation over repeated cycling. Meanwhile, the outermost carbon layer could inhibit the direct contact between Sn QDs and electrolyte to reduce the amount of irreversible SEI, leading to high Coulombic efficiency [17]. More strikingly, the Sn QDs@CNFs structure could offer a dramatically synergistic effect and thus enhance long-term electrochemical performance.

Furthermore, AC impedance analysis for the half cell was carried out to elucidate the charge and contact resistance of Sn QDs@CNFs electrode at selected cycle numbers, as plotted in **Figure 5d**. Interestingly, the impedance resistance of the Sn QDs@CNFs electrode decreased evidently after cycling. On the one hand, we attributed these impedance changes mainly to the unique composite structure of our electrodes. In contrast to the exposed Sn NPs, the electrolyte needs to penetrate into the outer thin carbon layer and then access the embedded Sn QDs, so the formation of SEI over the active Sn QDs should be gradual but steady. Once the stable formation of SEI was achieved, the electrical conductivity could be eventually established, and SEI cracking was also minimized due to the protection by the covered elastic carbon [38]. On the other hand, the lack of electrolyte wetting in the electrode materials before cycling also contributed to the result of decreased impedance. Similar behavior has also been reported on Sn-filled CNT [23],  $\text{Fe}_2\text{O}_3/\text{C}$  nanocomposites [38], and graphene foam@ $\text{Fe}_3\text{O}_4$  composite

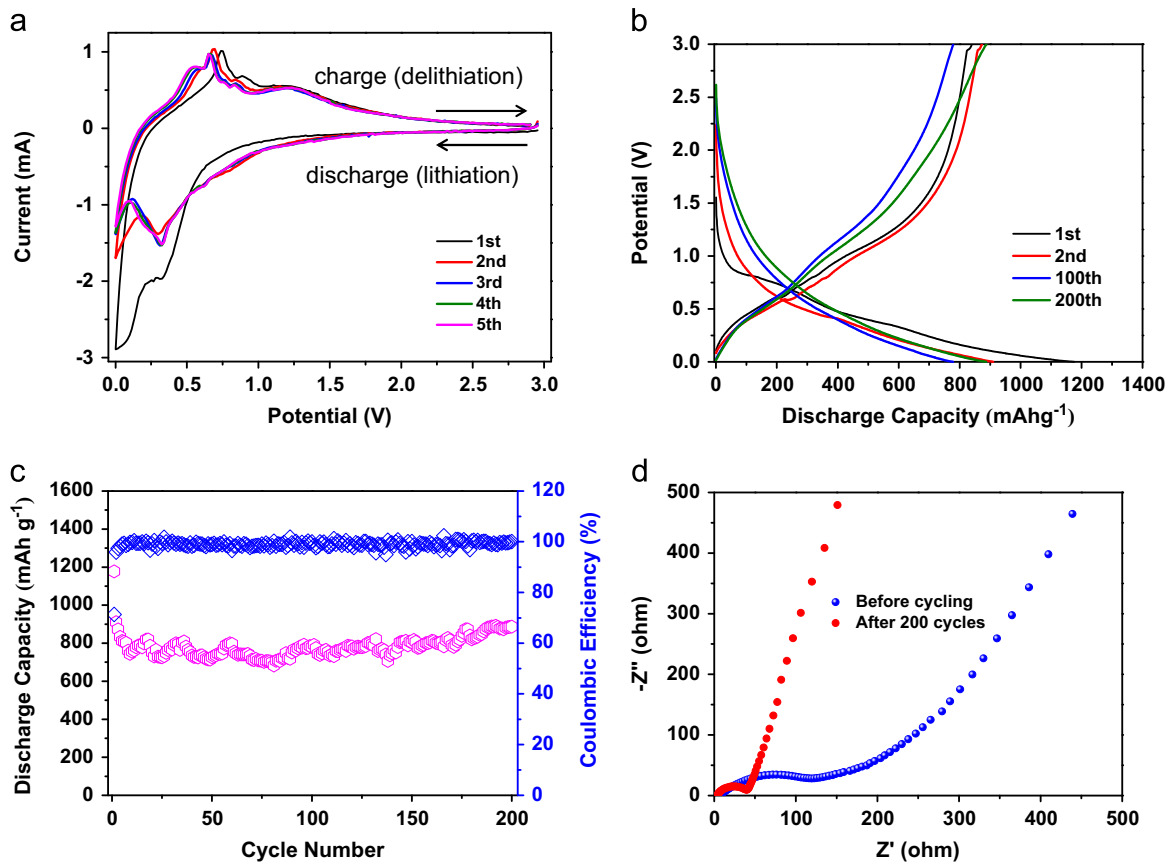


**Figure 5** (a) Typical CV curves of Sn QDs@CNFs electrode at  $0.5 \text{ mV s}^{-1}$  scanning rate. (b) Galvanostatic charge-discharge profiles of Sn QDs@CNFs electrode at a constant current density of  $0.1 \text{ A g}^{-1}$ . (c) Cycling performance and Coulombic efficiency of Sn QDs@CNFs electrode at  $0.1 \text{ A g}^{-1}$ . (d) Electrochemical impedance spectra of Sn QDs@CNFs electrode collected before (in blue) and after 200 cycles (in red) at  $0.1 \text{ A g}^{-1}$  in the frequency range from  $100 \text{ kHz}$  to  $0.01 \text{ Hz}$ .

anode materials [32] in LIBs. This result further explained why the discharge capacity gradually increased with the cycle number increasing. In addition, the Nyquist plots of Sn QDs@CNFs and N-doped CNFs electrode at fresh coin cells are shown in Figure S1. Obviously, the N-doped CNFs had a lower charge-transfer resistance, diffusion resistance, and Warburg impedance. As a consequence, the introduction of N-doped CNFs improved the conductivity and enhanced the electrochemical nature of Sn QDs.

To test the ultrafast charging and discharging capability of the electrodes, the galvanostatic discharge-charge measurements were carried out at  $0.2 \text{ A g}^{-1}$  and  $0.4 \text{ A g}^{-1}$ , respectively. The Sn QDs@CNFs electrode delivered an excellent discharge capability at different current densities, with an even more stable cycling performance, as shown in Figure 6. The Sn QDs@CNFs anode still displayed a large reversible capacity of about  $685 \text{ mAh g}^{-1}$  at  $0.2 \text{ A g}^{-1}$  after 500 cycles and  $508 \text{ mAh g}^{-1}$  at  $0.4 \text{ A g}^{-1}$  after 200 cycles, which corresponded to 74% and 67% retention of the initial discharge capacity, respectively. The rate performance is displayed in Figure S2, the Sn QDs@CNFs electrode could still deliver a reversible capacity of 463 and  $417 \text{ mAh g}^{-1}$  at the current density of  $0.88$  and  $1.32 \text{ A g}^{-1}$ , respectively. Even at  $2.22 \text{ A g}^{-1}$ , the reversible capacity maintained at  $371 \text{ mAh g}^{-1}$ , which was much higher than that of hard carbon [39], exhibiting excellent

rate capability. Such superior electrochemical performances were believed to result from the unique features with Sn QDs uniformly dispersed in the CNFs, as shown in Figure 6c. The superior rate capability should benefit from the N-doped carbon matrices with high electric conductivity and the porous carbon NFs structure, which could not only protect Sn but also provide fast and versatile transport pathways for the electrolyte ions during the electrochemical process. Moreover, the short diffusion path for both electrons and ions provided by the ultrasmall Sn particles further improved the rate performance. Besides, the cell capacity could remain stable even at high rate cycling, indicating that the unique structure of the composite could preserve the integrity of the electrode and thus tolerant to varied charge and discharge currents, which is important for high-power applications of rechargeable batteries.

## Conclusion

In conclusion, Sn QDs@CNFs composite with ultrasmall Sn QDs delicately dispersed in N-doped porous carbon matrices was prepared by electrospinning and further evaluated as an anode material for rechargeable Li-ion batteries. We demonstrated that as the anode of LIBs, Sn QDs@CNFs composite with the combination of ultrasmall Sn nanoparticles ( $<5 \text{ nm}$ ), uniform

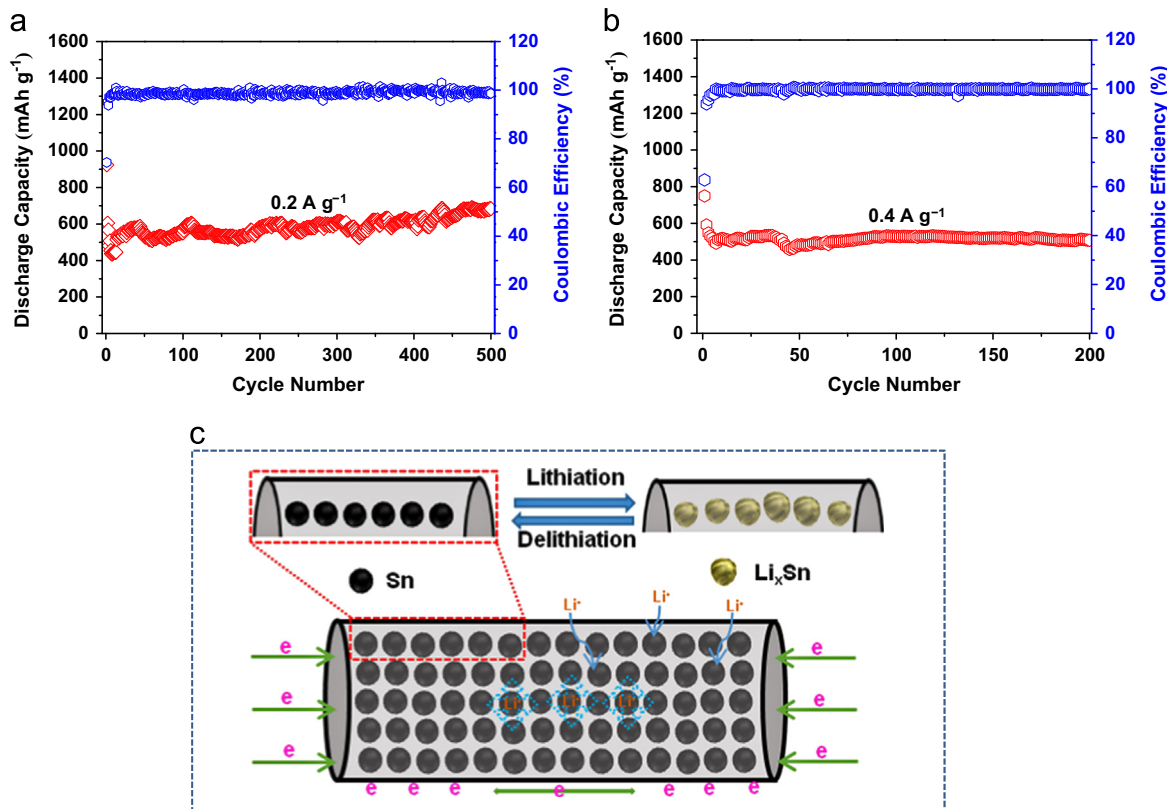


**Figure 6** Cycling performance of Sn QDs@CNFs electrode at (a)  $0.2 \text{ A g}^{-1}$  and (b)  $0.4 \text{ A g}^{-1}$ . (c) Schematic representation showing paths for lithium-ions and electrons in the Sn QDs@CNFs.

distribution and N-doped porous CNF structure rendered long cycling stability and high rate capability. At a current density of  $0.2 \text{ A g}^{-1}$ , a capacity of  $685 \text{ mAh g}^{-1}$  was maintained after 500 cycles. Even at much higher current density of  $2.22 \text{ A g}^{-1}$ , a reversible capacity of  $371 \text{ mAh g}^{-1}$  was obtained. These results would shed light on the practical application of Sn-based materials as a high capacity electrode with high rate capability for next-generation LIBs.

## Acknowledgments

We gratefully acknowledge the financial support from the National Natural Science Foundation of China (Grant nos. 11274107, 61204109, 21303046 and 21303047), the Program for New Century Excellent Talents in University (NCET-13-0185), and the Foundation for the authors of National Excellent Doctorial Dissertation of China (201318). Feng Li thanks the support from National Natural Science Foundation of China (Grant nos. 21071130 and 21371157) and Key Program of Henan Province for Science and Technology (132102210424). We also thank Dr. Yiqin Chen and Dr. Quan Xiang from Hunan University for XRD and Raman characterization.

## Appendix A. Supplementary materials

Supplementary data associated with this article can be found in the online version at <http://dx.doi.org/10.1016/j.nanoen.2014.06.030>.

## References

- [1] J. Hwang, S.H. Woo, J. Shim, C. Jo, K.T. Lee, J. Lee, ACS Nano 7 (2013) 1036-1044.
- [2] A. Magasinski, P. Dixon, B. Hertzberg, A. Kvist, J. Ayala, G. Yushin, Nat. Mater. 9 (2010) 353-358.
- [3] W.-M. Zhang, J.-S. Hu, Y.-G. Guo, S.-F. Zheng, L.-S. Zhong, W.-G. Song, L.-J. Wan, Adv. Mater. 20 (2008) 1160-1165.
- [4] Y. Idota, T. Kubota, A. Matsufuji, Y. Maekawa, T. Miyasaka, Science 276 (1997) 1395-1397.
- [5] J. Hassoun, G. Derrien, S. Panero, B. Scrosati, Adv. Mater. 20 (2008) 3169-3175.
- [6] K. Kravchyk, L. Protesescu, M.I. Bodnarchuk, F. Krumeich, M. Yarema, M. Walter, C. Guntlin, M.V. Kovalenko, J. Am. Chem. Soc. 135 (2013) 4199-4202.
- [7] Y. Qiu, K. Yan, S. Yang, Chem. Commun. 46 (2010) 8359-8361.
- [8] Z. Zhu, S. Wang, J. Du, Q. Jin, T. Zhang, F. Cheng, J. Chen, Nano Lett. 14 (2013) 153-157.
- [9] Y. Xu, Q. Liu, Y. Zhu, Y. Liu, A. Langrock, M.R. Zachariah, C. Wang, Nano Lett. 13 (2013) 470-474.
- [10] Y. Yu, L. Gu, C. Zhu, P.A. van Aken, J. Maier, J. Am. Chem. Soc. 131 (2009) 15984-15985.
- [11] K.T. Lee, Y.S. Jung, S.M. Oh, J. Am. Chem. Soc. 125 (2003) 5652-5653.
- [12] G. Derrien, J. Hassoun, S. Panero, B. Scrosati, Adv. Mater. 19 (2007) 2336-2340.
- [13] W.H. Shin, H.M. Jeong, B.G. Kim, J.K. Kang, J.W. Choi, Nano Lett. 12 (2012) 2283-2288.
- [14] Y. Zou, Y. Wang, ACS Nano 5 (2011) 8108-8114.
- [15] Q. Wei, Q. An, D. Chen, L. Mai, S. Chen, Y. Zhao, K.M. Hercule, L. Xu, A. Minhas-Khan, Q. Zhang, Nano Lett. 14 (2014) 1042-1048.
- [16] C. Zhang, H.B. Wu, Z. Guo, X.W.D. Lou, Electrochim. Commun. 20 (2012) 7-10.

- [17] L. Ji, Z. Tan, T. Kuykendall, E.J. An, Y. Fu, V. Battaglia, Y. Zhang, *Energy Environ. Sci.* 4 (2011) 3611-3616.
- [18] C. Chae, J.H. Kim, J.M. Kim, Y.-K. Sun, J.K. Lee, *J. Mater. Chem.* 22 (2012) 17870-17877.
- [19] B. Zhang, Y. Yu, Z. Huang, Y.-B. He, D. Jang, W.-S. Yoon, Y.-W. Mai, F. Kang, J.-K. Kim, *Energy Environ. Sci.* 5 (2012) 9895-9902.
- [20] Y. Yu, L. Gu, C. Zhu, P.A. van Aken, J. Maier, *J. Am. Chem. Soc.* 131 (2009) 15984-15985.
- [21] G. Zhang, H. Duan, B. Lu, Z. Xu, *Nanoscale* 5 (2013) 5801-5808.
- [22] Z. Wen, Q. Wang, Q. Zhang, J. Li, *Adv. Funct. Mater.* 17 (2007) 2772-2778.
- [23] X. Hou, H. Jiang, Y. Hu, Y. Li, J. Huo, C. Li, *ACS Appl. Mater. Interfaces* 5 (2013) 6672-6677.
- [24] J. Qin, C. He, N. Zhao, Z. Wang, C. Shi, E.-Z. Liu, J. Li, *ACS Nano* 8 (2014) 1728-1738.
- [25] B. Luo, B. Wang, X. Li, Y. Jia, M. Liang, L. Zhi, *Adv. Mater.* 24 (2012) 3538-3543.
- [26] Z.-S. Wu, W. Ren, L. Wen, L. Gao, J. Zhao, Z. Chen, G. Zhou, F. Li, H.-M. Cheng, *ACS Nano* 4 (2010) 3187-3194.
- [27] D.-J. Xue, S. Xin, Y. Yan, K.-C. Jiang, Y.-X. Yin, Y.-G. Guo, L.-J. Wan, *J. Am. Chem. Soc.* 134 (2012) 2512-2515.
- [28] N. Mahmood, C. Zhang, F. Liu, J. Zhu, Y. Hou, *ACS Nano* 7 (2013) 10307-10318.
- [29] G. Zhang, Y. Chen, B. Qu, L. Hu, L. Mei, D. Lei, Q. Li, L. Chen, Q. Li, T. Wang, *Electrochim. Acta* 80 (2012) 140-147.
- [30] J. Zhu, G. Zhang, X. Yu, Q. Li, B. Lu, Z. Xu, *Nano Energy* 3 (2014) 80-87.
- [31] I.S. Kim, P. Kumta, G. Blomgren, *Electrochem. Solid-State Lett.* 3 (2000) 493-496.
- [32] J. Luo, J. Liu, Z. Zeng, C.F. Ng, L. Ma, H. Zhang, J. Lin, Z. Shen, H.J. Fan, *Nano Lett.* 13 (2013) 6136-6143.
- [33] D. Wang, J. Yang, X. Li, D. Geng, R. Li, M. Cai, T.-K. Sham, X. Sun, *Energy Environ. Sci.* 6 (2013) 2900-2906.
- [34] P. Poizot, S. Laruelle, S. Grugeon, L. Dupont, J. Tarascon, *Nature* 407 (2000) 496-499.
- [35] P.-L. Taberna, S. Mitra, P. Poizot, P. Simon, J.-M. Tarascon, *Nat. Mater.* 5 (2006) 567-573.
- [36] S. Liang, X. Zhu, P. Lian, W. Yang, H. Wang, *J. Solid State Chem.* 184 (2011) 1400-1404.
- [37] D. Deng, J.Y. Lee, *J. Mater. Chem.* 20 (2010) 8045-8049.
- [38] X. Huang, H. Yu, J. Chen, Z. Lu, R. Yazami, H.H. Hng, *Adv. Mater.* 26 (2014) 1296-1303.
- [39] D. Kim, S.H. Kang, M. Slater, S. Rood, J.T. Vaughey, N. Karan, M. Balasubramanian, C.S. Johnson, *Adv. Energy Mater.* 1 (2011) 333-336.



**Guanhua Zhang** is a Ph.D. candidate of College of Physics and Microelectronics, Hunan University, under the supervision of Prof. Huigao Duan. Her main research interests include hierarchical nanomaterials for environmental and green energy applications such as lithium ion batteries and supercapacitors.



**Jian Zhu** received his B.S. degree from the college of Chemistry and Chemical Engineering at Hunan University in 2011. He is a Ph.D. candidate of Key Laboratory for Micro-Nano Optoelectronic Devices of Ministry of Education, Hunan University. His research interests include novel nanomaterials' preparation and application.



**Wei Zeng** received his B.S. degree from the college of Chemistry and Chemical Engineering at Hunan University in 2012. He is a Ph.D. candidate of Key Laboratory for Micro-Nano Optoelectronic Devices of Ministry of Education, Hunan University. His research interests focus on the novel nano-materials preparation and applications for green energy storage and conversion.



**Sucheng Hou** is a graduate student from the College of Microelectronics and Physics, Hunan University. His research is focused on the synthesis of 3D structure of metal oxide nanomaterials and their applications in LIBs and supercapacitors.



**Feilong Gong** is a Ph.D. candidate of Chemistry and Chemical Engineering for physical chemistry, XinJiang University. His major study focuses on controlling growth and gas sensors about hierarchical ZnO nanomaterial.



**Feng Li** is a Ph.D. of Chemical Sciences, Nanjing University. His major study focuses on new types of functional material, energy storage, sensor technology, and water treatment/purification technology. As the first author and corresponding author, he published more than 50 papers, such as *Angewandte Chemie International Edition*, *Journal of the American Chemical Society*, *Advanced Materials*, *Advanced Functional Materials*, *ACS Nano* and so on. He has undertaken many research projects, such as National Natural Science Foundation of China, National Water Special Corpus, Innovation Research Team, Outstanding Talents Project of Henan Province, Key Scientific and Technological Project of Henan Province and so on.



**Cheng Chao Li** received his Ph.D. degree from the School of Materials Science & Engineering, Hunan University in 2013 under the supervision of Prof. Taihong Wang. From 2008 to 2012, he was supported by CSC to conduct his research on nanomaterials synthesis and self-assembly as an exchange Ph.D. student in Prof. Hua Chun Zeng's group at National University of Singapore. Currently, he is working at School of Physics and Electronics, Hunan University. His research interest includes design and preparation of inorganic micro/nanostructures and their applications in energy storage such as Lithium ion batteries, supercapacitors and Li-oxygen batteries.



**Huigao Duan** received his B.S. degree (2004) and Ph.D. (2010) in Condensed Matter Physics from Lanzhou University, China. He is currently a Professor at the College of Physics and Microelectronics, and a member at the State Key Laboratory for Chemo/Biosensing and Chemometrics, Hunan University, China. From 2008 to 2010, he joined Research Laboratory of Electronics, MIT, as a Visiting Ph.D. Student. From 2010 to 2012, he worked as a staff Scientist in Institute of Materials Research and Engineering, A\*STAR in Singapore. He was also a visiting scientist in University of Stuttgart in 2012. His main research interests focus on sub-10-nm electron-beam lithography and its related applications in nanodevices.